Trans. of Korean Hydrogen and New Energy Society, Vol. 29, No. 6, 2018, pp. 559~569
DOI: https://doi.org/10.7316/KHNES.2018.29.6.559

KHNES
pISSN 1738-7264 • eISSN 2288-7407

무회분탄에 분산된 니켈 촉매의 톨루엔 수증기 개질

Lia Priscilla · 김수현 · 유지호† · 최호경 · 임영준 · 임정환 · 김상도 · 전동혁 · 이시훈

한국에너지기술연구원 청정연료연구실

Nickel Catalysts Supported on Ash-Free Coal for Steam Reforming of Toluene

LIA PRISCILLA, SOOHYUN KIM, JIHO YOO†, HOKYUNG CHOI, YOUNGJOON RHIM, JEONGHWAN LIM, SANGDO KIM, DONGHYUK CHUN, SIHYUN LEE

Clean Fuel Laboratory, Korea Institute of Energy Research, 152 Gajeong-ro, Yuseong-gu, Daejeon 34129, Korea

†Corresponding author : jyoo@kier.re.kr

Received 31 August, 2018
Revised 21 November, 2018
Accepted 30 December, 2018

Abstract >> Catalytic supports made of carbon have many advantages, such as high coking resistance, tailorable pore and surface structures, and ease of recycling of waste catalysts. Moreover, they do not require pre-reduction. In this study, ash-free coal (AFC) was obtained by the thermal extraction of carbonaceous components from raw coal and its performance as a carbon catalytic support was compared with that of well-known activated carbon (AC). Nickel was dispersed on the carbon supports and the resulting catalysts were applied to the steam reforming of toluene (SRT), a model compound of biomass tar. Interestingly, nickel catalysts dispersed on AFC, which has a very small surface area (~0.13 m^2/g), showed higher activity than those dispersed on AC, which has a large surface area (1,173 m^2/g). X-ray diffraction (XRD) analysis showed that the particle size of nickel deposited on AFC was smaller than that deposited on AC, with the average values on AFC ≈ 11 nm and on AC ≈ 23 nm. This proved that heteroatomic functional groups in AFC, such as carboxyls, can provide ion-exchange or adsorption sites for the nano-scale dispersion of nickel. In addition, the pore structure, surface morphology, chemical composition, and chemical state of the prepared catalysts were analyzed using Brunauer-Emmett-Taylor (BET) analysis, transmission electron microscopy (TEM), scanning electron microscopy (SEM), x-ray diffraction (XRD), Fourier-transform infrared (FT-IR) spectroscopy, and temperature-programmed reduction (TPR).

Key words : Ash-free coal(무회분탄), Steam reforming(수증기 개질), Nickel(니켈), Catalytic support(촉매 지지체), Carbon(탄소)

1. Introduction

Coal has been used as the main heat source in many industries, such as thermal power generation, iron smelting, and cement[1]. The organic components of coal include carbon (>70 wt%), oxygen, hydrogen, nitrogen, and sulfur. When coal is pyrolyzed, the heteroatomic groups present in it usually devolatilize and the carbon component becomes even more dominant[2]. This characteristic enables coal to be used as the raw material for various carbon materials, suchfor example catalytic support[3,4].

Most varieties of coal are rich in functional groups such as carboxyl, hydroxyl, and amines, where the nano-scale dispersion of metals can happen via ion exchange and/or adsorption[5]. The coal support is expected to have high coking resistance[6]. The dispersed metal exists in a reduced state due to the high reducing ability of the carbon support, so the reduction step required for the activation of reforming catalysts can be skipped[7]. The activity is tailorable by controlling the pore structure and surface properties[8]. It is easy to recycle the catalyst after use. However, coal contains inorganic ashes, which limit its usefulness to some extent.

Inorganic ashes that typically have a small surface area (<10 m^2/g) are unsuitable for the dispersion of metals. They might react with active metals irreversibly, deactivating the catalysts[9]. One of the most successful techniques for the removal of ashes in coal is thermal extraction, in which organic solvents are used to extract the carbonaceous components in coal, producing ash-free coal (AFC)[10,11]. In this study, AFC prepared by thermal extraction was evaluated as a catalytic support.

Activated carbon (AC) is a common example of carbon catalytic supports. Metals are dispersed on AC owing to its large surface area[12]. In this study, the dispersion of nickel on AFC containing surface functional groups is compared with the dispersion on AC with large Brunauer–Emmett–Taylor (BET) surface area[13].

Investigations into the utilization of biomass as carbon-zero energy sources have been actively conducted[14,15]. A large amount of sticky tar is generated during the combustion and gasification process, thereby reducing the overall efficiency of the system[16]. Several studies actively focus on methods to eliminate this tar. One of the major advances in this direction is the identification of tar waste as a hydrocarbon energy source, and its conversion to hydrogen via steam reforming[17,18]. Researchers have, so far, attained the required level of catalytic activity, but the severe coking that occurs typically causes the deactivation of the catalyst. Therefore, strategies to improve the longevity of these catalysts are the need of the hour. In this study, the catalytic activity of nickel catalysts prepared using carbon support (AFC and AC), which are known to have high coking resistance, was evaluated for use in the steam reforming of toluene (SRT), one of the major components of tar[19,20].

In the work, nickel was dispersed on carbon supports (AFC and AC) by either wet impregnation (Imp) or simple incipient wetness impregnation (IWI) method, and their effect on the performance was evaluated[21,22]. Also, the physical and chemical characteristics of prepared catalysts were analyzed using BET analysis, transmission electron microscopy (TEM), scanning electron microscopy (SEM), x-ray diffraction (XRD), Fourier-transform infrared (FT-IR) spectroscopy, and temperature-programmed reduction (TPR).

2. Experimental

2.1 Materials

AFC was produced using Indonesian low rank coal (Kideco) as raw coal and N-methyl-2-pyrrolidone (NMP) as the organic solvent. The AFC was extracted at 350°C and 30 bar. A detailed description can be found elsewhere[23]. AC (obtained from coconut shell by steam activation) having 1,173 m^2/g surface area was obtained from Shinkwang Chemical Ind. Co. Ltd. Results of the proximate and ultimate analysis of the supports are tabulated in Table 1.

2.2 Preparation of catalysts

Nickel was dispersed either by wet impregnation (Imp) or incipient wetness impregnation method (IWI). For Imp, the nickel precursor in either methanol or dimethylformamide (DMF) was mixed with the support powder (<200 μm)[10]. The Imp samples in Table 2 were prepared using methanol-based process other than 24.4 Ni/AFC-Imp (DMF-based). Then, the pH of the solution was adjusted to ~9 by adding ammonia and the solution was stirred for 6 hours prior to washing and overnight drying. The dried sample was then calcined at 650°C for 30 minutes under N_2. For IWI, a nickel precursor solution was dropped with mild mixing to wet the support until the support became fully wet, which was then dried overnight. In Table 2, 14.9 Ni/AC-IWI was prepared using the precursor in methanol and 15.8 Ni/AC-IWI using that in H_2O. The impregnated support was pyrolyzed at the same conditions as for Imp. In total, four AFC-supported and three AC-supported catalysts were prepared (Table 2). The metal loading was determined by inductively coupled plasma-mass spectrometer (ICP-MS).

The nomenclature of the catalyst samples is as follows: the number in the catalyst name indicates the loading of nickel metal and the dispersion method (Imp or IWI) is mentioned after the hyphen; for example, 11.8 Ni/AFC-Imp represents the nickel catalyst having a Ni loading of 11.8 wt%, dispersed on AFC by the Imp method.

Table 1. Proximate/ultimate analysis of AFC and AC

Sample	Proximate analysis (wt.%)				Ultimate analysis (wt.%) daf				
	M	VM*	FC*	Ash*	C	H	N	O	S
AFC	4.8	56.9	41.8	1.3	75.1	6.4	4.8	13.6	0.1
AC	4.0	5.9	91.6	2.5	97.8	0.5	1.7	0.0	0.0

M, moisture; VM, volatile matter; FC, fixed carbon; daf, dry & ash-free.
*Dry basis.

Table 2. Features of the synthesized catalyst samples

Name	Support	Method	Ni loading (wt%)
11.8 Ni/AFC-Imp	AFC	Imp	11.8
13.2 Ni/AFC-IWI		IWI	13.2
17.4 Ni/AFC-Imp		Imp	17.4
24.4 Ni/AFC-Imp		Imp	24.4
1.8 Ni/AC-Imp	AC	Imp	1.8
14.9 Ni/AC-IWI		IWI	14.9
15.8 Ni/AC-IWI			15.8

2.3 Catalytic activity test

A detailed description of the test is given in the previous report[10]. A brief overview of the test method is as follows. The steam reforming of 1,000 ppm toluene was done in a fixed bed reactor. The catalyst (0.1 g) was placed on quartz wool supported by a quartz frit placed in the middle of a quartz reactor (ID=1 cm). Toluene in N_2 (100 mL/min) was mixed with steam and delivered to the reactor. Steam was produced by the evaporation of water in a heated stainless steel tubing (150°C). Steam re-

forming was done at 400°C and GHSV= 8,000 hr^{-1}.

The generated gas (H_2, CH_4, CO, and CO_2) was quantified using gas chromatography (GC, Agilent 6890). Carbon conversion and hydrogen yield were calculated according to (Eq. 1) and (Eq. 2), respectively;

$$\text{Conversion}\,(\%) = \frac{([CO_2]_{out} + [CO]_{out} + [CH_4]_{out})}{(7 \times [\text{toluene}]_{in})} \times 100 \quad \text{(Eq.1)}$$

$$H_2\ \text{yield}\,(\%) = \frac{[H_2]_{out}}{(18 \times [\text{toluene}]_{in})} \times 100 \quad \text{(Eq.2)}$$

2.4 Instrumental analysis

Proximate analysis was performed based on the ASTM D5142 standard using a TGA-701 thermogravimeter (LECO Co., USA), while elemental analysis was performed using CHN-2000 Elemental Analyzer (LECO Co., USA). ICP-MS was conducted to determine the nickel loading of the catalysts using an X-series ICP/MS (Thermo Scientific, USA). TEM images were obtained using a Tecnai G2-20 S-twin TEM (FEI Company, USA). SEM images were obtained using S-4800 (Hitachi, Japan). The chemical composition was characterized using DMax 2500PC XRD (Rigaku, Japan). Fourier-transform infrared spectroscopy (FT-IR) measurements were carried out using a Nicolet 6700 (Thermo Electron Scientific Inc., USA). H_2 temperature-programmed reduction (H_2 TPR) was done using a Belcat-Basic (BEL Inc., Japan). The samples were pretreated with Ar (50 mL/min) at 150°C for 30 minutes prior to analysis and then reduced using 10% H_2 in Ar (30 mL/min) with the temperature increasing from 50 to 900°C (5°C/min ramp rate).

3. Results and Discussion

3.1 Characterization of Ni/AFC and Ni/AC catalysts

The BET surface area and pore characteristics of AFC and AC supports were determined using the N_2 adsorption-desorption isotherms.

According to the International Union of Pure and Applied Chemistry (IUPAC) classification, AC shows a pore structure that is mainly composed of micropores with minor mesopores and the pore size distribution over a broad region (Fig. 1, Table 3)[24]. It has a large surface area (1,173 m^2/g), showing potential as a good support for the fine dispersion of metals.

The BET surface area of as-prepared AFC is very

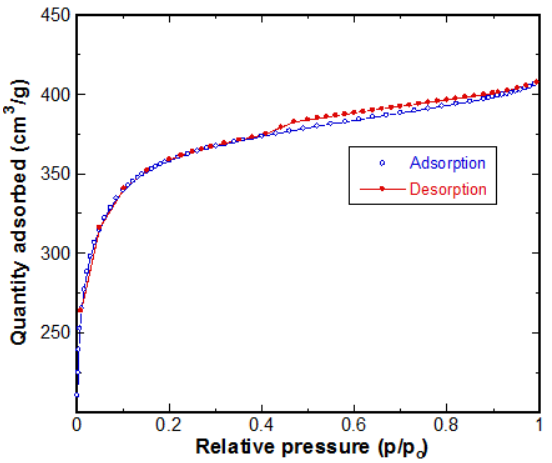

Fig. 1. N_2 adsorption-desorption isotherms of AC

Table 3. Pore characteristics of AFC and AC

Catalytic support	SA (m^2/g)	V_{total} (cm^3/g)	V_{micro} (cm^3/g)	D_p (nm)
AFC	0.13	3.4×10^{-4}	4.3×10^{-5}	108.3
AC	1173	0.52	0.48	17.8

SA, BET surface area; V_{total}, total pore volume; V_{micro}, micropore volume; D_p, average pore diameter.

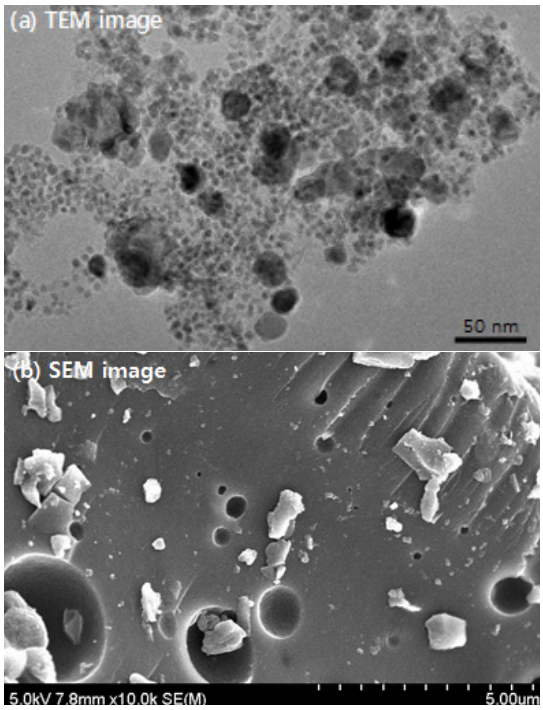

Fig. 2. (a) TEM image of 24.4 Ni/AFC-Imp and (b) SEM image of 24.4 Ni/AFC-Imp

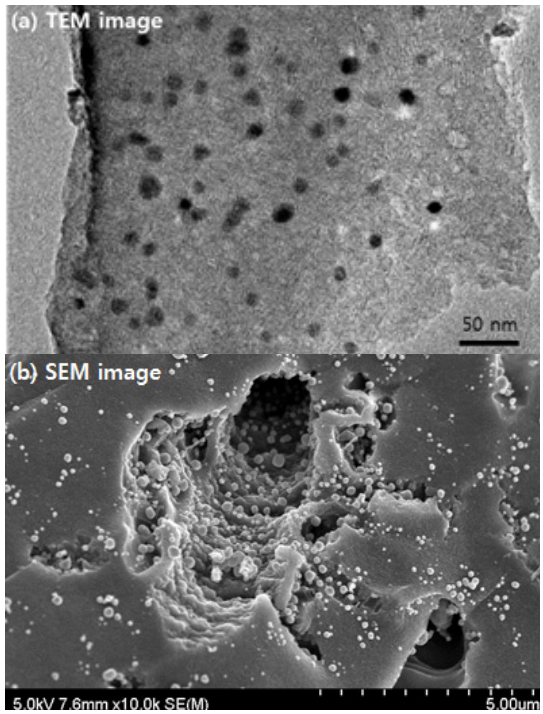

Fig. 3. (a) TEM image of 14.9 Ni/AC-IWI and (b) SEM image of 14.9 Ni/AC-IWI

small (0.13 m^2/g) and therefore, is not plotted in Fig. 1. The N_2 adsorption isotherm of the AFC-supported catalyst was not readily measurable. The melting-solidifying transition experienced during the ramp up to 650°C probably resulted in the removal of pores[25]. Previous studies showed that pore blocking due to the dispersion of nickel on the coal support is minor[26].

Four different nickel catalysts supported on AFC were prepared by either Imp or IWI method; 11.8 Ni/AFC-Imp, 13.2 Ni/AFC-IWI, 17.4 Ni/AFC-Imp, and 24.4 Ni/AFC-Imp (Table 2). TEM image of the 24.4 Ni/AFC-Imp catalyst shows the nickel dispersed on the AFC support (Fig. 2[a]).

Non-uniform distribution of nickel particles, which have particle size less than 20 nm, on the AFC can be observed. Smaller nickel particles (mostly less than 5 nm) were found on the low rank coal (LRC) supports[10]. The oxygen content of LRC is more than 20 wt%, AFC has relatively low oxygen content (13.7 wt%) (Table 1). This means that the number of ion exchange and adsorption sites in the AFC support is less than in LRC and as a result, larger particles are formed. The SEM image (Fig. 2[b]) shows a continuous, smooth, and glassy surface morphology. The AFCs, which generally have high thermoplasticity, were probably melted at ~300°C and re-solidified by further heating to 650ºC (pyrolysis temperature)[25]. This melting seemingly led to a compact and smooth surface. LRC-supported catalysts have a bubble-like porous surface, which is different from AFC-supported ones[26].

TEM image of an AC-supported nickel catalyst is given in Fig. 3(a).

The discrete nickel particles have sizes ~20 nm. Compared to the AFC-supported catalyst that con-

tained numerous nickel particles, a relatively small number of such particles are found on the AC-supported catalyst. The oxygen functional groups in AFC (Table 1) probably play an important role on the metal dispersion via either the ion-exchange mechanism or adsorption[11,27]. As a result, 24.4 Ni/AFC-Imp has better metal dispersion than 14.9 Ni/AC-IWI. All three AC-supported samples (Table 2) were made using a nickel nitrate precursor to take advantage of its high solubility and decomposition at moderate temperature. However, it is known that the thermal decomposition of the nitrate form is difficult to control, resulting in poorly dispersed nickel particles[28]. The surface of AC appears to consist of stacked layers with many small ellipsoidal particles and numerous holes (Fig. 3[b]).

3.2 SRT using Ni/AFC and Ni/AC catalysts

Toluene is converted to hydrogen and carbon dioxide via steam reforming (Eq. 3) and water-gas shift reaction (Eq. 4).

$$C_7H_8 + 7H_2O \rightarrow 11H_2 + 7CO \quad \text{(Eq. 3)}$$

$$CO + H_2O \leftrightarrow H_2 + CO_2 \quad \text{(Eq. 4)}$$

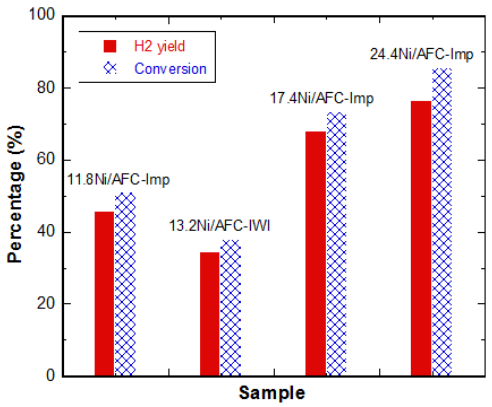

Fig. 4. Catalytic activity of nickel supported on AFC for SRT

Performance of the catalysts was evaluated in terms of hydrogen yield (Eq. 1) and carbon conversion (Eq. 2).

Four catalysts supported on AFC were made with different nickel loading (11.8, 13.2, 17.4, and 24.4 wt% Ni) and dispersion methods (Imp and IWI) (Table 2). The extent of their catalytic activities are summarized in Fig. 4.

Both hydrogen yield and carbon conversion of the AFC-supported catalysts increased with nickel loading for the samples prepared by wet impregnation method (Imp); 24.4 Ni/AFC-Imp gave ~76% H_2 yield, 17.4 Ni/AFC-Imp ~68%, and 11.8 Ni/AFC-Imp ~45%. The sample with the highest nickel loading (24.4 Ni/AFC-Imp) was synthesized using the same procedure as for 11.8 Ni/AFC-Imp. The only difference was the solvent used for dissolution of the precursor; dimethylformamide (DMF) for 24.4 Ni/AFC-Imp and MeOH for 11.8 Ni/AFC-Imp. Compared to MeOH, DMF seems to have a better affinity to AFC[29]. Therefore, higher nickel loading as well as catalytic activity was obtained[30]. However, the high metal loading might render the material more susceptible to metal sintering[31]. The sample prepared by IWI (13.2 Ni/AFC-IWI) showed ~10% lower H_2 yield than 11.8 Ni/AFC-Imp. This lower activity despite the higher nickel loading indicates that the Imp method might be more efficient than IWI with regard to the metal dispersion on AFC support. AFC support showed better performance than LRC support for the SRT reaction[10]. The fine nickel particles (<5 nm) were uniformly present on LRC support, most likely due to the large amount of oxygen functional groups that serve as seeds for the dispersion. This can provide more reaction sites. Nonetheless, the higher catalytic activity of AFC-supported nickel suggests that the kinetics of SRT is also affected by factors other than the chemical reaction.

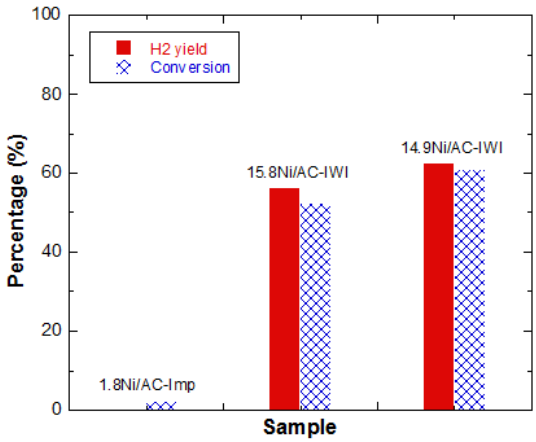

Fig. 5. Catalytic activity of nickel supported on AC for SRT

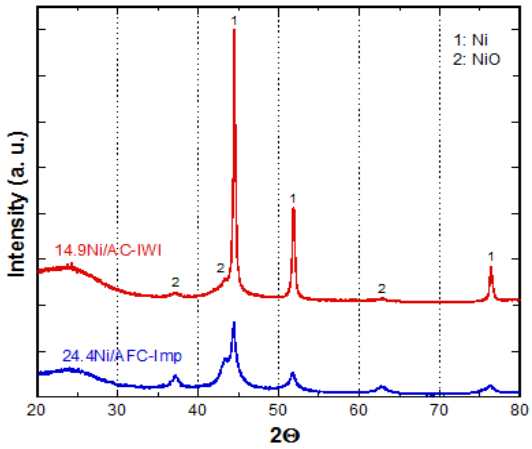

Fig. 6. XRD patterns of 24.4 Ni/AFC-Imp and 14.9 Ni/AC-IWI

Three AC-supported nickel catalysts were prepared; 1.8 Ni/AC-Imp, 15.8 Ni/AC-IWI, and 14.9 Ni/AC-IWI (Table 2). Their performance is shown in Fig. 5.

The target metal loading (~15 wt% as metal basis) was not obtained by Imp method in the AC support. Since AC was made at an elevated temperature (~800ºC), heteroatomic functional groups, which served as seeds for the metal dispersion, were mostly devolatilized and therefore, AC was composed mostly of carbon (97.8 wt%) (Table 1). This probably caused the low metal loading (1.8 wt%) for 1.8 Ni/AC-Imp, giving less than 3% carbon conversion. On the other hand, the target loading was obtained when dispersed by IWI. 15.8 Ni/AC-IWI was prepared using an aqueous solution of nickel precursor and 14.9 Ni/AC-IWI using MeOH solution. H_2 yields of the two samples were similar (~60%) and the difference was within the reproducibility range (±5%), indicating that the effect of the precursor solution (H_2O and MeOH) during the IWI process was minor. The difference in catalytic activity between the AC and AFC supports is not directly comparable, since they were made under different conditions. However, AFC combined with Imp method looks favorable for better SRT reaction (Figs. 4, 5).

3.3 XRD, FT-IR, and TPR analysis

XRD patterns of 24.4 Ni/AFC-Imp and 14.9 Ni/AC-IWI are shown in Fig. 6.

General XRD patterns were comparable for the two samples. Both nickel metal and NiO peaks were observed; Ni peaks at 2θ=44.5°, 51.9°, and 76.4°[31] and NiO peaks at 2θ=37.3°, 43.3°, and 62.9°[32,33]. Broad peaks at 2θ<30º correspond to the non-crystalline carbon phase[34]. The efficient contact of nickel species with the carbon support induces the reduction of the metal due to the oxidation propensity of carbon[35]. However, the NiO/Ni peak intensity ratio was relatively high for 24.4 Ni/AFC-Imp. This might be due to the relatively high nickel loading; some of the nickel particles were not in good contact with the AFC support and were agglomerated in the oxide form. On the other hand, the Ni metallic peak was dominant in 14.9 Ni/AC-IWI. According to the Scherrer equation that relates the size of particles to the peak width, broader peaks from the AFC than from the AC sample in-

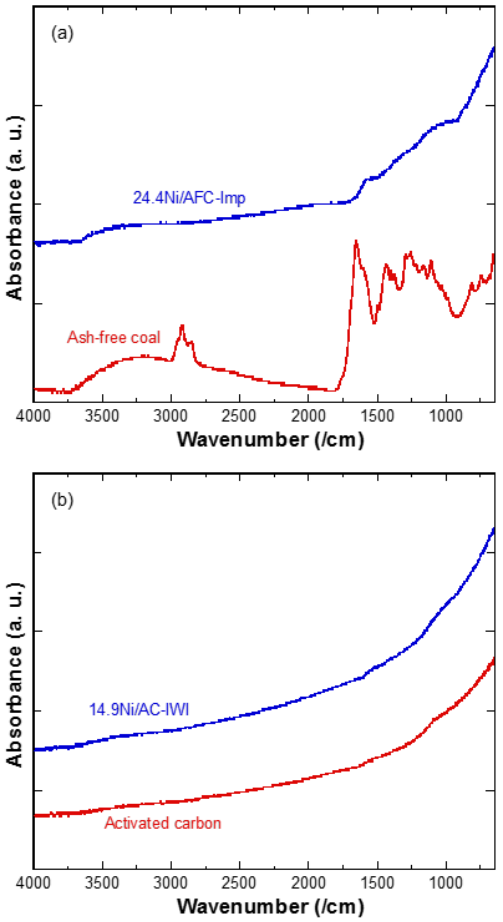

Fig. 7. FT-IR spectra of (a) AFC and 24.4 Ni/AFC-Imp, and (b) AC and 14.9 Ni/AC-IWI

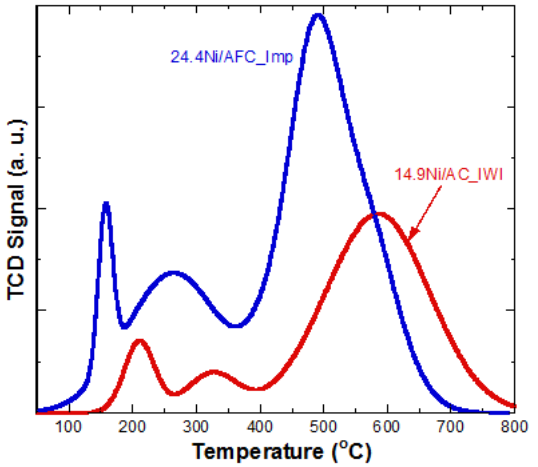

Fig. 8. H_2-TPR profiles of 24.4 Ni/AFC-Imp and 14.9 Ni/AC-IWI catalyst

dicate that the average size of the nickel particles was smaller when supported by AFC (~11 nm) than AC (~23 nm)[36]. Peaks due to silica ash were not observed for both the catalysts, establishing that the ash content was less than 3 wt%[37,38].

FT-IR spectra were obtained for the supports and the catalysts made using them in order to determine the surface functional groups (Fig. 7).

The spectra of the AFC and AC supports were very different. Many peaks were clearly seen on the AFC spectrum: a broad –OH vibration peak between 3,600 and 3,000 cm^{-1}, aliphatic C−H peaks at ~2,850, ~1,470, and ~1,260 cm^{-1}, a strong carbonyl peak at ~1,700 cm^{-1}, an aromatic C=C peak at ~1,600 cm^{-1}, a conjugated C=O peak at 1,650 cm^{-1}, phenol (or ether) vibration peaks at 1,440 cm^{-1} and 1,200 cm^{-1}, and aromatic C−H peaks at 700-850 cm^{-1} [39-42]. The spectral pattern of 24.4 Ni/AFC-Imp was much reduced and very different from the AFC itself. Many functional groups were devolatilized during the pyrolysis at 650°C after metal dispersion. In contrast, a smooth line with no significant peaks was observed for AC. As shown in the ultimate analysis (Table 1), AC is lacking in the main components of the functional groups, such as oxygen and nitrogen. A similar FT-IR profile was observed for 14.9 Ni/AC-IWI. Ni particles were dispersed on AC via adsorption rather than ion exchange[43,44]. The adsorption was apparently strong enough to survive the pyrolysis at 650°C after the impregnation[45,46]. As shown in Fig. 6, the smaller nickel particles on AFC even with a BET surface area <1 m^2/g BET than on AC with large BET surface area (1,173 m^2/g) indicate that the oxygen functional groups of AFC enhanced the nickel metal dispersion (Table 1).

The metal-support interaction of 24.4 Ni/AFC-Imp and 14.9 Ni/AC-IWI was evaluated based on

the results of H_2 TPR (Fig. 8).

The AFC-supported catalyst (24.4 Ni/AFC-Imp) showed three reduction peaks at ~150°C (α peak), ~275°C (β peak), and ~500°C (γ peak). The broad γ peak indicated that strongly interacting NiO-AFC was dominant, followed by bulk NiO (α peak) and moderately interacting NiO (β peak)[47]. The AC-supported catalysts (14.9 Ni/AC-IWI) also exhibited three main peaks at 200°C (α peak), 350°C (β peak), and 600°C (γ peak). The peak intensity was followed the order β<α<γ, meaning that a main peak corresponded to the strong NiO-AC interaction, followed by bulk NiO and moderate NiO-AC interaction. The overall TPR profile showed that the metal-support interaction of NiO-AC is stronger than that of NiO-AFC[48]. The reduction peaks of 24.4 Ni/AFC-Imp at the lower temperatures imply that it can be reduced more easily than 14.9 Ni/AC-IWI[49]. The reduction at the lower temperature may be result of better nickel dispersion that enhances the reactivity of oxide metal toward reduction[50]. This bears out the broader XRD peak of 24.4 Ni/AFC-Imp than 14.9 Ni/AC-IWI (Fig. 6). Oxygen functional groups that exist on the AFC surface might also increase the reducibility of the nickel metal[51,52]. In addition, stronger TPR peaks of 24.4 Ni/AFC-Imp were probably the results of the higher NiO concentration than 14.9 Ni/AC-IWI, as evident from the XRD results (Fig. 6)[53,54].

4. Conclusions

Catalysts were made by dispersing nickel particles on AFC that was obtained by removing inorganic ashes from LRC, and tested for use in the SRT reaction, as toluene is a model compound of biomass tar. Although AFC has a very small surface area (<1 m^2/g), better nano-dispersion of nickel was observed on AFC (average particle size, ~11 nm) than on the AC support (average particle size, ~23 nm), which has a large surface area (1,173 m^2/g). The ion exchange and adsorption in AFC could be attributed to the oxygen and nitrogen functional groups present in it. The better dispersion of nickel probably contributed to the higher SRT activity of AFC-supported catalysts compared with the AC- supported ones. According to the XRD results, both AFC and AC supports acted as reducing agents, and thus, the dispersed nickel was present mainly in a metallic state, despite the absence of the pre-reduction step. TPR results showed that the interaction of nickel with the AFC support was weaker than that with AC. In the future, it is necessary to understand the catalytic performance of AFC support taking into consideration the metal-support interaction as well as the surface and pore structures.

Acknowledgements

This work was conducted under the framework of the Research and Development Program of the Korea Institute of Energy Research (KIER) (B8-2463-02).

References

1. H. H. Schobert, "Lignites of North America", Elsevier, The Netherlands, 1995.
2. J. Yu, J. A. Lucas, and T. F. Wall, "Formation of the structure of chars during devolatilization of pulverized coal and its thermoproperties: A review", Prog. Energy Combustion Sci., Vol. 33, 2007, pp. 135-170.
3. A. Ahmadpour and D. D. Do, "The preparation of active carbons from coal by chemical and physical activation", Carbon, Vol. 34, 1996, pp. 471-479.
4. C. Z. Li, "Some recent advances in the understanding of the pyrolysis and gasification behavior of Victorian brown coal", Fuel, Vol. 86, 2007, pp. 1664-1683.
5. M. Arif, F. Jones, A. Barifcani, and S. Iglauer, "Influence of surface chemistry on interfacial properties of low to high

rank coal seams", Fuel, Vol. 194, 2017, pp. 211-221.
6. F. Rodriguez-Reinoso, "The role of carbon materials in heterogeneous catalysis", Carbon, Vol. 36, 1998, pp. 159-175.
7. S. Kim, D. Chun, Y. Rhim, J. Lim, S. Kim, H. Choi, S. Lee, and J. Yoo, "Catalytic reforming of toluene using a nickel ion-exchanged coal catalyst", Int. J. Hydrogen Energy, Vol. 40, 2015, pp. 11855-11862.
8. P. Serp and J. L. Figuiredo, "Carbon Materials for Catalysis", John Wiley & Sons, Inc., USA, 2009.
9. S. Samih and J. Chaouki, "Catalytic ash free coal gasification in a fluidized bed thermogravimetric analyzer", Powder Technol., Vol. 316, 2017, pp. 551-559.
10. T. Yoshida, T. Takanohashi, K. Sakanishi, I. Saito, M. Fujita, and K. Mashimo, "The effect of extraction condition on 'HyperCoal' production (1) - Under room-temperature filtration", Fuel, Vol. 81, 2002, pp. 1463-1469.
11. T. Yoshida, C. Li, T. Takanohashi, A. Matsumura, S. Sato, and I. Saito, "Effect of extraction condition on 'HyperCoal' production (2) - Effect of polar solvents under hot filtration", Fuel Process. Technol., Vol. 86, 2004, pp. 61-72.
12. H. Jüntgen, "Activated carbon as catalyst support", Fuel, Vol. 65, 1986, pp. 1436-1446.
13. W. Mohd and A. Wan, "Textural characteristics, surface chemistry and oxidation of activated carbon", J. Nat. Gas Chem., Vol. 19, 2010, pp. 267-279.
14. R. Saidur, E. A. Abdelaziz, A. Demirbas, M. S. Hossain, and S. Mekhilef, "A review on biomass as a fuel for boilers", Renewable Sustainable Energy Reviews, Vol. 15, 2011, pp. 2262-2289.
15. J. A. Ruiz, M. C. Juárez, M. P. Morales, P. Muñoz, and M. A. Mendívil, "Biomass gasification for electricity generation: Review of current technology barriers", Renewable Sustainable Energy Reviews, Vol. 18, 2013, pp. 174-183.
16. J. Rizkiana, G. Guan, W. B. Widayatno, X. Hao, W. Huang, A. Tsutsumi, and A. Abudula, "Effect of biomass type on the performance of cogasification of low rank coal with biomass at relatively low temperatures", Fuel, Vol. 134, 2014, pp. 414-419.
17. Y. Shen and K. Yoshikawa, "Recent progresses in catalytic tar elimination during biomass gasification or pyrolysis - A review", Renewable Sustainable Energy Reviews, Vol. 21, 2013, pp. 371-392.
18. X. Liu, X. Yang, C. Liu, P. Chen, X. Yue, and S. Zhang, "Low-temperature catalytic steam reforming of toluene over activated carbon supported nickel catalysts", J. Taiwan Inst. Chem. Eng., Vol. 65, 2016, pp. 233-241.
19. J. A. Rached, C. E. Hayek, E. Dahdah, C. Gennequin, S. Aouad, H. L. Tidahy, J. Estephane, B. Nsouli, A. Aboukaïs, and E. Abi-Aad, "Ni based catalysts promoted with cerium used in the steam reforming of toluene for hydrogen production", Int. J. Hydrogen Energy, Vol. 42, 2017, pp. 1289-12840.
20. S. A. Benson and E. A. Sondreal, "Ash-related issues during combustion and gasification, in impact of mineral impurities in solid fuel combustion", Springer, USA, 1999, pp. 1-21.
21. H. D. Setiabudi, C. C. Chong, S. M. Abed, L. P. Teh, and S. Y. Chin, "Comparative study of Ni-Ce loading method: Beneficial effect of ultrasonic-assisted impregnation method in CO_2 reforming of CH_4 over Ni-Ce/SBA-15", J. Environ. Chem. Eng., Vol. 6, 2018, pp. 745-753.
22. E. Río, D. Gaona, J. C. Hernández-Garrido, J. J. Calvino, M. G. Basallote, M. J. Fernández-Trujillo, J. A. Perez-Omil, and J. M. Gatica, "Speciation-controlled incipient wetness impregnation : A rational synthetic approach to prepare sub-nanosized and highly active ceria–zirconia supported gold catalysts", J. Catal., Vol. 318, 2014, pp. 119-127.
23. I. Lee, S. Jin, D. Chun, H, Choi, S. Lee, K. Lee, and J. Yoo, "Ash-free coal as fuel for direct carbon fuel cell", Sci. China Chem., Vol. 57, 2014, pp. 1010-1018.
24. M. Thommes, K. Kaneko, A. V. Neimark, J. P. Olivier, F. Rodriguez-Reinoso, J. Rouquerol, and K. S. W. Sing, "Physisorption of gases, with special reference to the evaluation of surface area and pore size distribution (IUPAC Technical Report)", Pure Appl. Chem., Vol. 87, 2015, pp. 1051-10691.
25. T. Takanohashi, T. Shishido, H. Kawashima, and I. Saito, "Characterisation of HyperCoals from coals of various ranks", Fuel, Vol. 87, 2008, pp. 592-598.
26. N. Ruhswurmova, S. Kim, J. Yoo, D. Chun, Y. Rhim, J. Lim, S. Kim, H. Choi, and S. Lee, "Nickel supported on low rank coal for steam reforming of ethyl acetate", Int. J. Hydrogen Energy, Vol. 43, 2018, pp. 15880-15890.
27. R. A. Ortega-domínguez, H. Vargas-Villagrán, C. Peñaloza-Orta, K. Saavedra-Rubio, X. Bokhimi, and T. E. Klimova, "A facile method to increase metal dispersion and hydrogenation activity of Ni/SBA-15 catalysts", Fuel, Vol. 198, 2017, pp. 110-122.
28. E. Marceau, M. Che, J. Cejka, and A. Zukal, "Nickel (II) nitrate vs. acetate: Influence of the precursor on the structure and reducibility of Ni/MCM-41 and Ni/Al-MCM-41 catalysts", ChemCatChem, Vol. 2, 2010, pp. 413-422.
29. S. Murov, "Properties of organic solvents", Miller's Home, https://sites.google.com/site /miller00828/in/solvent-polarity-table, 1998.
30. D. Wierzbicki, R. Baran, R. Debek, M. Motak, T. Grzybek, M. E. Galvez, and P. Da, "The influence of nickel content on the performance of hydrotalcite-derived catalysts in CO_2 methanation reaction", Int. J. Hydrogen Energy, Vol. 42, 2017, pp. 23548-23555.

31. T. Van Haasterecht, M. Swart, K. P. De Jong, and J. H. Bitter, "Effect of initial nickel particle size on stability of nickel catalysts for aqueous phase reforming", J. Energy Chem., Vol. 25, 2016, pp. 289-296.
32. M. Wu, F. Chen, Y. Lai, and Y. Sie, "Electrocatalytic oxidation of urea in alkaline solution using nickel/nickel oxide nanoparticles derived from nickel-organic framework", Electrochim. Acta, Vol. 258, 2017, pp. 167-174.
33. M. Hu, M. Laghari, B. Cui, B. Xiao, B. Zhang, and D. Guo, "Catalytic cracking of biomass tar over char supported nickel catalyst", Energy, Vol. 145, 2018, pp. 228-237.
34. H. Takagi, K. Maruyama, N. Yoshizawa, Y. Yamada, and Y. Sato, "XRD analysis of carbon stacking structure in coal during heat treatment", Fuel, Vol. 83, 2004, pp. 2427-2433.
35. E. Auer, A. Freund, J. Pietsch, and T. Tacke, "Carbons as supports for industrial precious metal catalysts", Appl. Catal. A: General, Vol. 173, 1998, pp. 259-271.
36. S. A. Speakman, "Estimating crystallite size using XRD", MIT, Center for Materials Science and Engineering, USA, 2012.
37. B. L. Dutrow and C. M. Clark, "X-ray Powder Diffraction (XRD)", Carleton College, USA, 2008.
38. J. A. Newman, P. D. Schmitt, S. J. Toth, F. Deng, S. Zhang, and G. J. Simpson, "Parts per million powder X-ray diffraction", Anal. Chem., Vol. 87, 2015, pp. 10950-10955.
39. H. Xueqiu, L. Xianfeng, N. Baisheng, and S. Dazhao, "FTIR and Raman spectroscopy characterization of functional groups in various rank coals", Fuel, Vol. 206, 2017, pp. 555-563.
40. K. Wang, F. Du, and G. Wang, "The influence of methane and CO_2 adsorption on the functional groups of coals: Insights from a Fourier transform infrared investigation", J. Nat. Gas Sci. Eng., Vol. 45, 2017, pp. 358-367.
41. W. Geng, T. Nakajima, H. Takanashi, and A. Ohki, "Analysis of carboxyl group in coal and coal aromaticity by Fourier transform infrared (FT-IR) spectrometry", Fuel, Vol. 88, 2009, pp. 139-144.
42. B. Tian, Y. Qiao, Y. Tian, K. Xie, Q. Liu, and H. Zhou, "FTIR study on structural changes of different-rank coals caused by single/multiple extraction with cyclohexanone and NMP/CS_2 mixed solvent", Fuel Process. Technol., Vol. 154, 2016, pp. 210-218.
43. M. Karnib, A. Kabbani, H. Holail, and Z. Olama, "Heavy metals removal using activated carbon, silica and silica activated carbon composite", Energy Procedia, Vol. 50, 2014, pp. 113-120.
44. J. C. Moreno-Pirajan and L. Giraldo, "Heavy metal ions adsorption from wastewater using activated carbon from orange peel", E-Journal Chem., Vol. 9, 2012, pp. 926-937.
45. G. S. Miguel, S. D. Lambert, and N. J. D. Graham, "Thermal regeneration of granular activated using inert atmospheric conditions", Environ. Technol., Vol. 23, 2002, pp. 1337-1346.
46. B. Ledesma, S. Román, A. Álvarez-murillo, E. Sabio, and J. F. González, "Cyclic adsorption/thermal regeneration of activated carbons", J. Anal. Appl. Pyrolysis, Vol. 106, 2014, pp. 112-117.
47. S. He, Z. Mei, N. Liu, and L. Zhang, "Ni/SBA-15 catalysts for hydrogen production by ethanol steam reforming : Effect of nickel precursor", Int. J. Hydrogen Energy, Vol. 42, 2017, pp. 14429-14438.
48. R. da P. Fiuza, M. A. de Silva, and J. S. Boaventura, "Development of Fe-Ni/YSZ-GDC electrocatalysts for application as SOFC anodes: XRD and TPR characterization and evaluation in the ethanol steam reforming reaction", Int. J. Hydrogen Energy, Vol. 35, 2010, pp. 11216-11228.
49. S. Yeqin, Z. Ying, L. Hanfeng, Z. Zekai, and C. Yinfei, "Soot combustion performance and H_2-TPR study on ceria-based mixed oxides", Chinese J. Catal., Vol. 34, 2013, pp. 567-577.
50. S. D. Robertson, B. D. McNicol, H. H. De Baas, S. C. Kloet, and J. W. Jenkins, "Determination of reducibility and identification of alloying in copper-nickel-on-silica catalysts by temperature-programmed reduction", J. Catal., Vol. 37, 1975, pp. 424-431.
51. B. F. Machado and P. Serp, "Graphene-based materials for catalysis", Catal. Sci. Technol., Vol. 2, 2012, pp. 54-75.
52. J. Chen and S. Wu, "Acid/base-treated activated carbons: characterization of functional groups and metal adsorptive properties", Langmuir, Vol. 20, 2004, pp. 2233-2242.
53. Z. Li, G. Zhou, C. Li, and T. Cheng, "Effect of Pr on copper-based catalysts for ethane oxychlorination", Catal. Commun., Vol. 40, 2013, pp. 42-46.
54. M. Luo, P. Fang, M. He, and Y. Xie, "In situ XRD, Raman, and TPR studies of CuO/Al_2O_3 catalysts for CO oxidation", J. Mol. Catal. A Chem., Vol. 239, 2005, pp. 243-248.